The Influence of Protonation States on the Dynamics of the NhaA Antiporter from *Escherichia coli*

Elena Olkhova,* Etana Padan,† and Hartmut Michel*

*Department of Molecular Membrane Biology, Max Planck Institute of Biophysics, D-60438 Frankfurt am Main, Germany; and †Department of Biological Chemistry, Alexander Silberman Institute of Life Sciences, Hebrew University of Jerusalem, Jerusalem 91904, Israel

ABSTRACT The crystal structure of NhaA Na^+/H^+ antiporter of *Escherichia coli* has provided a basis to explore the mechanism of Na^+ and H^+ exchange and its regulation by pH. However, the dynamics and nature of the pH-induced changes in the proteins remained unknown. Using molecular mechanics methods, we studied the dynamic behavior of the hydrogen-bonded network in NhaA on shifting the pH from 4 to 8. The helical regions preserved the general architecture of NhaA throughout the pH change. In contrast, large conformational drifts occurred at pH 8 in the loop regions, and an increased flexibility of helix IVp was observed on the pH shift. A remarkable pH-induced conformational reorganization was found: at acidic pH helix X is slightly curved, whereas at alkaline pH, it is kinked around residue Lys^{300}. The barrier that exists between the cytoplasmic and periplasmic funnels at low pH is removed, and the two funnels are bridged by hydrogen bonds between water molecules and residues located in the TMSs IV/XI assembly and helix X at alkaline pH. In the variant $Gly^{338}Ser$ that lost pH control, a hydrogen-bonded chain between Ser^{338} and Lys^{300} was found to block the pH-induced conformational reorganization of helix X.

INTRODUCTION

Sodium-proton antiporters are essential enzymes that catalyze the exchange of sodium ions for protons across cytoplasmic and organelle membranes of many different origins (1–3). NhaA is the main Na^+/H^+ antiporter of *Escherichia coli* and many other enterobacteria (2). It is inactive at pH 7 and below but is maximally active at pH 8.5 (4). Regulation of antiport activity by pH is a common property of many Na^+/H^+ antiporters. The pH regulation requires a ''pH sensor'' whose change in protonation leads to conformational alterations in different parts of the protein that transduce the pH signal into a change in activity (5). NhaA is electrogenic with a stoichiometry of two H^+ exchanged for one Na^+ (4).

The crystal structure of NhaA, in the down-regulated conformation found at pH 4, has recently been determined at 3.45 Å resolution (6) (Fig. 1). NhaA contains 12 transmembrane segments (TMSs). Two negatively charged funnels (cytoplasmic and periplasmic) point to each other but are separated by a group of densely packed hydrophobic residues creating a barrier between the funnels. The cytoplasmic funnel formed of TMSs II, IX, IVc (**p** and **c** stand for the periplasmic and cytoplasmic parts of the respective helices), and V opens to the cytoplasm and ends in the middle of the membrane at the putative ion binding site (Fig. 1). The periplasmic funnel formed by TMSs II, VIII, and XIp opens toward the periplasm. The TMS IV and TMS XI are interrupted by extended chains that cross each other. This TMSs IV/XI assembly creates a delicately balanced electrostatic environment in the middle of the membrane. The ''pH sensor'' appears to be located at the cytoplasmic funnel entry and to transduce the pH signal (at alkaline pH) to the TMSs IV/XI assembly to activate the antiporter (6).

The physical separation between the pH sensor and the exchange machinery revealed by the structure entails long-range pH-induced conformational changes for pH activation, as observed in both prokaryotic and eukaryotic Na^+/H^+ antiporters (5,7,8). On the basis of the x-ray structure, it has been proposed that binding of the charged substrates causes an electrostatic imbalance, allowing for a rapid alternating access to the binding sites (6), the mechanism of the cation exchange. Although the crystal structure of NhaA provides many clues to the understanding of the ion-translocation mechanism and its pH regulation, the questions of the nature of the pH-induced conformational change and the dynamics of this process remain unanswered. In addition, the x-ray crystallographic structure determination did not allow the identification of bound water molecules because the resolution was not high enough. Therefore, in our previous in silico study, water molecules were introduced using the GRID method (9), and the initial hydrogen-bonded network of NhaA was ruled out (10). We also described the effect of pH titration on the protonation states of titratable residues in NhaA and the influence of explicit internal hydration on the electrostatic interactions in the antiporter and calculated the protonation states of all titratable residues in NhaA using the multi-conformation continuum electrostatics (MCCE) method (11). Biochemical studies showed that activation of NhaA by a pH shift is accompanied by a conformational change as probed by a monoclonal antibody (12) and by accessibility of NhaA to trypsin (13) or MIANS, a fluorescent probe (14). However,

Submitted September 26, 2006, and accepted for publication January 17, 2007.

Address reprint requests to Elena Olkhova, Max Planck Institute of Biophysics, Max-von-Laue Str., 3, D-60438 Frankfurt am Main, Germany. Tel.: 49-69-6303-1056; Fax: 49-69-6303-1002; E-mail: Elena.Olkhova@mpibp-frankfurt.mpg.de.

0006-3495/07/06/3784/08 $2.00

doi: 10.1529/biophysj.106.098269

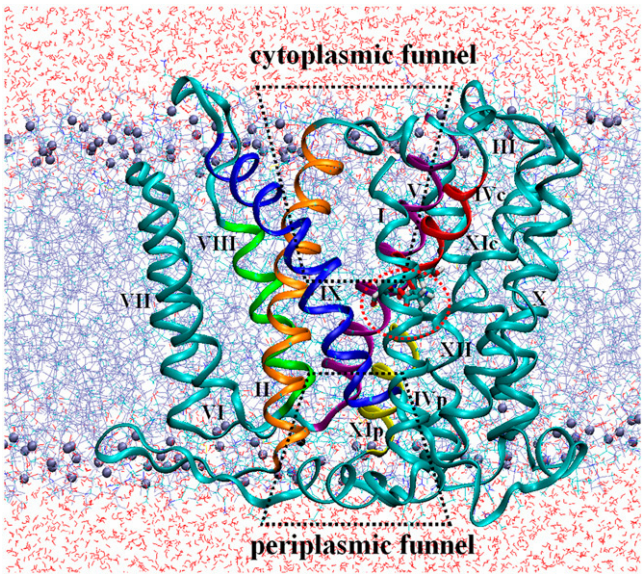

FIGURE 1 The overall structure of the NhaA molecule represented as a ribbon model embedded in a DMPC membrane solvated by a 100 mM NaCl aqueous salt solution (NhaA molecule shown in *green*, DMPC lipids are shown in *ice-blue*, head groups of lipids are shown in *blue*, water molecules are shown in *red*). The snapshot was taken at the beginning of the MD production for the simulation at pH 4. A negatively charged funnel formed of TMSs II (shown in *orange*), IX (shown in *blue*), IVc (shown in *red*), and V (shown in *purple*) opens to the cytoplasm and ends in the middle of the membrane at the putative ion-binding site. In TMS IV and TMS XI the helices are interrupted by extended chains that cross each other. This TMSs IV/XI assembly creates a delicately balanced electrostatic environment in the middle of the membrane. A shallow negatively charged funnel formed by TMSs II (shown in *orange*), VIII (shown in *green*), and XIp (shown in *yellow*) opens to the periplasm. Image was prepared with VMD (26).

these approaches monitored steady-state conditions and could not follow the dynamics of the change in the protein.

Hence, a clearer understanding of the structural reorganization of NhaA requires elucidation of the dynamic conformational changes occurring in response to pH shifts. Molecular dynamics (MD) simulation provides a powerful tool for computational investigations of protein conformational changes and the possibility of examining the initial events leading to the activation of the antiporter.

Here, we study the dynamic behavior of the hydrogen-bonded network in NhaA at acidic and alkaline pH. We generate and analyze data from two 4-ns-long MD simulations of the wild-type NhaA Na^+/H^+ antiporter and the G338S variant, a constitutively active variant lacking the pH regulation, embedded in an explicit lipid bilayer. The work focuses mainly on determining the effect of pH on the structural reorganization of the NhaA antiporter.

THEORY AND METHODS

Coordinates

The atomic model was derived from crystallographic data obtained under cryoconditions of the NhaA Na^+/H^+ antiporter from *Escherichia coli* at 3.45 Å resolution, Protein Data Bank entry 1ZCD (6). NhaA consists of 388 amino acid residues with the N- and C-termini exposed to the cytoplasm. The structural model comprises residues 9–384, which are arranged in 12 transmembrane segments (6). Na^+ ions and water molecules could not be identified at the available resolution. The N- and C-termini residues were modeled using the CHARMM software package (version c28b2) (15). The protonation states of residues in NhaA had been calculated previously (10) using the MCCE (multiconformation continuum electrostatics) method. Charges on the protein atoms and ionizable groups in different protonation states were taken from the CHARMM22 force field (16,17). Previous MCCE calculations suggested that Asp^{133} is in its neutral state over a wide pH range (pH 4–15) (10). However, based on the structure, it has been postulated to compensate the partial positive charges at the N-terminal ends of helices IVc and XIp (6). Therefore, in our simulations Asp^{133} was kept as a deprotonated negatively charged residue.

Initial setup of the simulated systems

Parallel simulations with different protonation states of NhaA antiporter at pH 4 (PH4 set of coordinates) and at pH 8 (PH8 set of coordinates), 4.0 ns each in length, were carried out under conditions of constant temperature and pressure using three-dimensional periodic boundary conditions (PBC) and full electrostatics. A proper membrane environment for NhaA was provided by constructing a dimyristoylphosphatidylcholine (DMPC) lipid bilayer. We used the general protocol for MD simulations (18,19) to construct the initial configuration of a protein-membrane-water system. The microscopic system consists of NhaA Na^+/H^+ antiporter (384 residues), 200 DMPC lipids (98 in the top and 102 in the bottom layer), and bulk water molecules (9,214 molcules for the PH4 set of coordinates and 9,233 molcules for the PH8 set of coordinates). Additionally, 54 internal water molecules positioned using the GRID method (10) were included in the calculations at low and high pH. Na^+ and Cl^- ions were inserted to simulate a 150 mM aqueous salt solution (263 Na^+ and 286 Cl^- ions for the PH4 set and 263 Na^+ and 268 Cl^- ions for the PH8 set). After solvation the entire systems consisted of 57,670 atoms (PH4 set of coordinates) and 57,660 atoms (PH8 set of coordinates), respectively. The $Gly^{338}Ser$ (G338S) mutation was made to the embedded structure at pH 8 by replacing the residue Gly^{338} by Ser using the molecular modeling software InsightII (LC) (Accelrys, San Diego, CA). The total simulation system consisted of 57,664 atoms (PH8-G338S set of coordinates). Periodic boundary conditions were applied in the *xy* directions to simulate an infinite planar layer and in the *z* direction to simulate a bilayer system; the periodic system has the dimensions $90 \times 90 \times 100$ Å^3.

Equilibration and dynamics

The minimization and dynamics simulations were performed using the academic version c28b2 of the biomolecular simulation package CHARMM (15). Equilibraion and dynamics procedures were adopted from Berneche and colleagues (18,19).

The simulations were performed under three-dimensional PBC. The total length of the equilibration procedure was 670 ps for both PH4 and PH8 systems. The systems were first coupled to a heat bath at 330 K by the use of Langevin dynamics at constant volume; the time steps were 2 fs. The last 270 ps of the equilibration and the production was at constant pressure of 1.0 atm and a temperature of 330 K (19). In the first part of the equilibration, harmonic restraints (applied to the center of mass of the polar head groups, the protein backbone, and the ions) were gradually decreased to allow a smooth relaxation of the system (20). The coordinates were saved every 10 ps, and the nonbonded and image lists were updated every 20 steps. The list of nonbonded interactions was truncated at 12 Å, using an atom-based cutoff. The nonbonded van der Waals interaction was switched off at 10–12 Å. The electrostatic interactions were computed without truncation, using the particle mesh Ewald (PME) algorithm (21) with an order of 4, and FFT grid points for the charge mesh per angstrom were $90 \times 90 \times 100$. In the PME method implemented in CHARMM, the electrostatic energy was split

into a direct and a reciprocal Ewald sum. A real-space Gaussian-width κ of 0.3 $Å^{-1}$ was used. All bonds involving hydrogen atoms were constrained by applying the SHAKE algorithm (22). The all-atom potential energy functions PARAM-22 for protein (16,17) and phospholipids (23) were used. The TIP3P potential was used for the water molecules (24). During the production trajectory the center of mass of the protein was restrained to the center of the *xy* plane. The overall simulation time was 4.0 ns for both PH4 and PH8 systems.

To evaluate the distortion of TM helix X, we applied a computational algorithm ProKink (25). This method can describe the three-dimensional geometry of the distortion in a helix; the structural features of a hinge in the helix can be characterized by the bend and wobble angles, which can be defined in terms of a prehinge helix and a posthinge helix similarly to the characterization of proline kinks. The bend angle is the angle between the two parts of the helix when it is bent along its axis. It ranges from 0° to 180°; the closer its value to 0°, the smaller is the bend in the helix. The wobble angle is the angle that defines the orientation of the posthinge helix in respect to the prehinge helix. It ranges from −180° to 180°. The wobble angle is close to 0° when the axis of the posthinge helix is bent so that its axis is moved toward the Cα atom of the hinge residue, and it is close to ±180° when it is moved away from the hinge. The wobble angle is negative when the posthinge helix axis has a negative *z* value, and it is positive for positive values of *z*.

Hydrogen bonds

The hydrogen bond patterns were analyzed from the production trajectories with 0.2-ps time resolution. The criteria for a hydrogen bond (A. . .H–D) were that the distance between the acceptor and the hydrogen atom (A. . .H) was less than 2.5 Å and that the A. . .H–D angle was more than 120° (26). The percentage of occupancy of a hydrogen bond was defined as the number of frames with the hydrogen bond present divided by the total number of frames used for analysis. The average lifetime of a hydrogen bond during the simulation was then calculated as the average of all of its occurrences excluding those with a lifetime shorter than 1 ps. We consider here only hydrogen bonds with occupancies of more than 10%.

Root mean-square deviations and atomic fluctuations

The coordinate sets from every 0.2 ps of the production run were superimposed on the initial structure of the system by minimizing the mass-weighted root mean-square deviations (RMSD) of the heavy atoms from the initial structure. The average RMSD values of the Cα atoms, side chains, and some amino acids were then calculated for the entire MD trajectory. B-factors (Debye-Waller factor) from the x-ray structure of NhaA were compared with the atomic fluctuations (RMSF) in the simulations.

Computational details

Energy minimization, membrane modeling, and MD simulations were performed in parallel with 16 processors, using version c28b2 of the biomolecular simulation program CHARMM (15) on an IBM RS/6000 PS5 Regatta supercomputer at the Max Planck Society Rechenzentrum in Garching. All molecular structures were drawn using the Visual Molecular Dynamic Software VMD 1.8 (27).

RESULTS AND DISCUSSION

Average structural properties

To measure the degree of conformational drift from the initial structure, we have analyzed the RMSDs of the backbone atoms from the starting structure of the antiporter at pH 4 and pH 8 (Fig. 2 *A*). At 330 K, the backbone RMSD over the first 1.5 ns is ~2.5 Å, regardless of the protonation states of titratable residues in NhaA (e.g., similar at pH 4 and at pH 8). At the end of the MD production, the RMSDs for simulations at pH 8 are substantially higher than those for the simulations at pH 4. This result means that the structure is much better preserved in the simulation at low pH. Interestingly, if only the α-helical regions are considered, the RMSD value for the simulation set at pH 4 is only 1.7 Å, and for the simulation set at pH 8 is only 1.4 Å after 2.0 ns of dynamics production (Fig. 2 *B*). However, the α-helical RMSDs after 2.5 ns are ~1.7 Å for both pH values. This result indicates that at pH 8 the greater structural drift in the simulated system is largely a result of conformational changes occurring in the loop regions.

Identification of the pH-induced conformational changes

To evaluate the flexibility of the different regions of NhaA at different pH values and to identify the regions of the protein

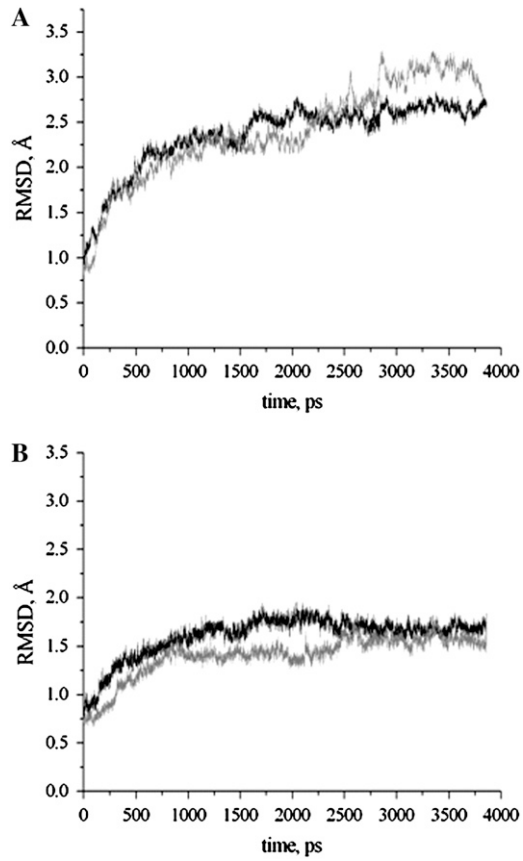

FIGURE 2 Atom-positional root mean-square deviations (RMSD) of the backbone atoms of the antiporter calculated from the MD production trajectories at pH 4 (*black line*) and at pH 8 (*gray line*) (*A*). RMSD values calculated only for the α-helices of the protein (*B*).

that undergo the largest motions, we calculated the RMSFs of each Cα atom from its time-averaged coordinates (Fig. 3). The overall RMSF for each simulation shows higher RMSFs for the loops and lower RMSFs for the cores of the helices. Helices I, II, IVc, V, VI, VII, VIII, XI, and XII were stable over the simulations at pH 4 and at pH 8 (Fig. 3).

Yet, the simulations show interesting features of TMS IV, which in the crystal structure does not form a continuous helix but is interrupted by residues Thr^{132} and Asp^{133} to form separate helices IVp (residues 121–131) and IVc (residues 134–143) (Fig. 4, *A* and *B*). Helix IVp has higher RMSFs than helix IVc at alkaline pH as opposed to acidic pH, where these two helices have a very slight difference in RMSFs. The RMSFs of helix IVp are larger at alkaline pH as compared with acidic pH (Fig. 3). However, no significant conformational reorganization of the helix is seen in the structure at pH 8 (Fig. 4, *A* and *B*). Therefore, we suggest that helix IVp displays an increased flexibility. Notably, the high flexibility observed for loop III–IV (residues 117–120, Fig. 3) may facilitate such motions of helix IVp, but we do not observe any significant motion for residues Thr^{132} and Asp^{133}. The pH-induced fluctuations revealed in helix IVp are consistent with the pH-induced conformational changes that have recently been detected by electron crystallographic studies on two-dimensional crystals of the NhaA Na^+/H^+ antiporter (M. Appel and W. Kühlbrandt, Max Planck Institute of Biophysics, Frankfurt am Main, personal communication, 2007) showing differences in the respective area between projection maps at pH 4 versus pH 8.

Most interestingly, we found significantly higher RMSF values for helix X, formed by residues 290–311, at alkaline pH when compared with acidic pH (Fig. 3). The schematic representation of the pH-dependent movement of this helix shows that in contrast to a slightly curved shape at pH 4, helix X exists in a kinked configuration at pH 8 (Fig. 4 *A*).

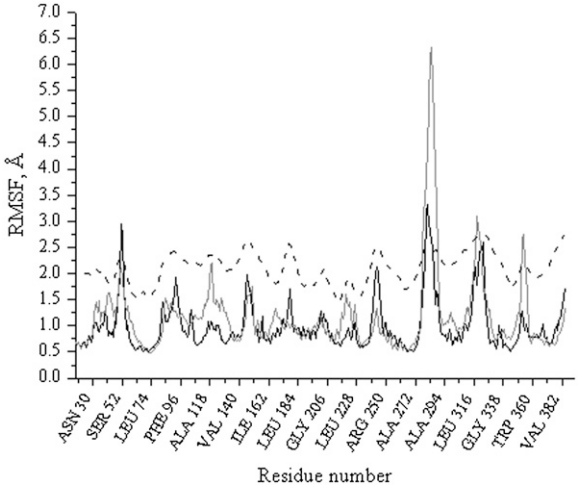

FIGURE 3 RMSFs of the backbone atoms calculated from the experimental B-factor (*black dashed line*) and from the dynamic trajectories for the simulations at pH = 4 (*black line*) and at pH = 8 (*gray line*). All values are averaged over the individual amino acids.

Analysis of the x-ray structure of NhaA suggests that there is a bend at the center of helix X with the central hinge point at the residue Gly^{299}, which precedes residues Lys^{300} and Pro^{301}. The ability of helices to kink was observed for many membrane proteins (for review see Luecke (28)) and has been correlated to the membrane protein functions (29–31). The structural features of a hinge were characterized by two parameters, the bend and wobble angles, which were defined in terms of a prehinge helix and posthinge helix similarly to the analysis of proline kinks (31) (Fig. 4 *B*). These refer to the part of the helix from the residue Leu^{290} to the hinge residue Gly^{299} and to the part from the hinge residue Gly^{299} to the residue Ala^{311}, respectively. Fig. 4 *C* depicts the temporal development of the bend and wobble angles for the helix X of NhaA during MD production runs at pH 4 and at pH 8. The value of the bend angle after the first 2.0 ns was ~45° regardless of the pH value. At the end of simulations, helix X displays a larger bend angle of ~58° at pH 8 compared with pH 4 in which the bend angle was ~23°. Additionally, the orientation of the posthinge helix differs in the simulations at low and high pH. The wobble angle in the end of simulation at low pH was ~−130°, whereas in the simulation at high pH, it was −50°. Any observed discrepancy may be caused by a different protonation state of Lys^{300} at high pH. Conformational reorganization of helix X at pH 8 results in a close proximity of helix X, helix XII, and helix IVp. The reference distance between the Cα atoms of Gly^{368} in helix XII and of Lys^{300} in helix X is only 5.7 Å, whereas for the simulations at pH 4, it is 7.2 Å. The distance between the Cα atoms of Asp^{133} (in the extended chain between helix IVp and helix IVc) and of Lys^{300} in helix X also becomes smaller, from 12.6 Å at low pH to 12.0 Å at high pH. Thus, helix X does not behave as a rigid α-helix on activation of the antiporter at alkaline pH, but as two rigid α-helical segments connected by a central hinge, the movement of which is pH dependent.

Water as a structural element

Under physiological conditions, the NhaA Na^+/H^+ antiporter catalyzes the import of two protons from the periplasm into the cytoplasm and the export of one sodium ion per cycle. This process contributes to the maintenance of a rather constant intracellular pH in *Escherichia coli* of ~7.6 at more alkaline extracellular pH values, and to the excretion of surplus sodium ions, which are toxic to the cell (reviewed by Padan et al. (3,5)). This fact implies that protons must have access to the sodium-binding site, most likely via water molecules located in the cytoplasmic and periplasmic funnels. We have therefore calculated the variation of the number of water molecules present in the cytoplasmic and periplasmic funnels and the variation in the number of hydrogen bonds formed between these water molecules and the protein residues at pH 4 and pH 8.

For these calculations, we considered at the *z* axis of the molecule the following residues: Glu^{252} located in the

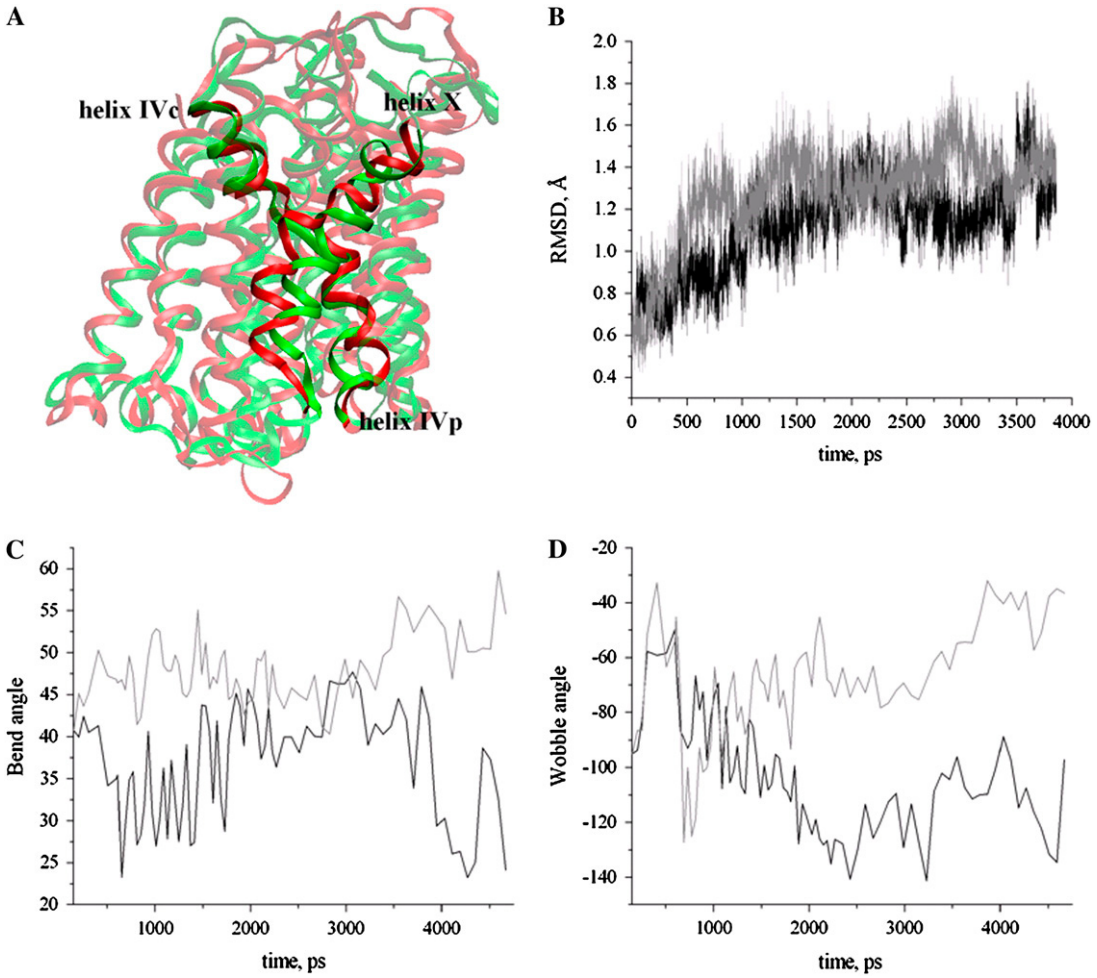

FIGURE 4 Superimposition of the NhaA antiporter atomic models at pH 4 and at pH 8 after 4.0 ns of MD production. (*A*) Structure at pH 4 is shown in green; the structure at pH 8 is shown in red. (*B*) RMSFs of the backbone atoms of helix X at pH 4 (*black line*) and at pH 8 (*gray line*). Bend (*C*) and wobble (*D*) angles of the inner helix X as a function of the simulation time during equilibration procedure and dynamics production at pH 4 (*black line*) and at pH 8 (*gray line*).

entrance of the cytoplasmic funnel, Asp^{133} and Asp^{163} located at the end of this funnel at the putative sodium binding site in the middle of the membrane, Asp^{65} located at the rim of the periplasmic funnel, and Lys^{57} located in its entrance. We have characterized the hydrogen-bonded interactions between the protein residues and water molecules based on the definition of the hydrogen bond as a geometrical construct from the MD trajectories during the simulations at pH 4 and at pH 8 (Fig. 5). It is obvious that the overall hydrogen-bonded network in the antiporter is quite different at low and high pH. At pH 4 the hydrophobic barrier in the middle of the membrane is clearly seen. The two negatively charged funnels are separated by a hydrophobic barrier of ~12 Å, as measured between two water oxygen atoms in the hydration shell of Asp^{163} and Lys^{300} in the acidic pH down-regulated antiporter (Fig. 5). No water molecules were found to cross this barrier from trajectory analyses of simulations at low pH. Remarkably, at pH 8, the hydrophobic barrier is removed, and two funnels are bridged by hydrogen bonds between water molecules and residues Asp^{133}, Asp^{163}, Tyr^{261}, and Cys^{335}. This means that water molecules diffuse into the barrier. For example, residue Asp^{133} forms a stable hydrogen bond with a water molecule W_G9 (modeled GRID water) with a high occupancy (66%), and the distance between Asp^{133} and Asp^{65} narrows down to only ~7 Å (Fig. 5 *B*) as a result of reorientation of the site chain of Asp^{65} in the simulation at high pH. This structural relocation of the charged residue Asp^{65} into the nonpolar hydrophobic barrier in the simulations under alkaline conditions is associated with penetration of water into the hydrophobic region and, hence, increases the local polarizability of the antiporter. This observation means that the internal electrostatics of the antiporter strongly influences the penetration of water molecules into the interior of NhaA.

Our results also show the most interesting hydrogen-bonded connections among residues of the putative Na^+ binding site, water molecules, and Lys^{300} of helix X. In the simulations at pH 4, Asp^{163} forms a hydrogen bond with

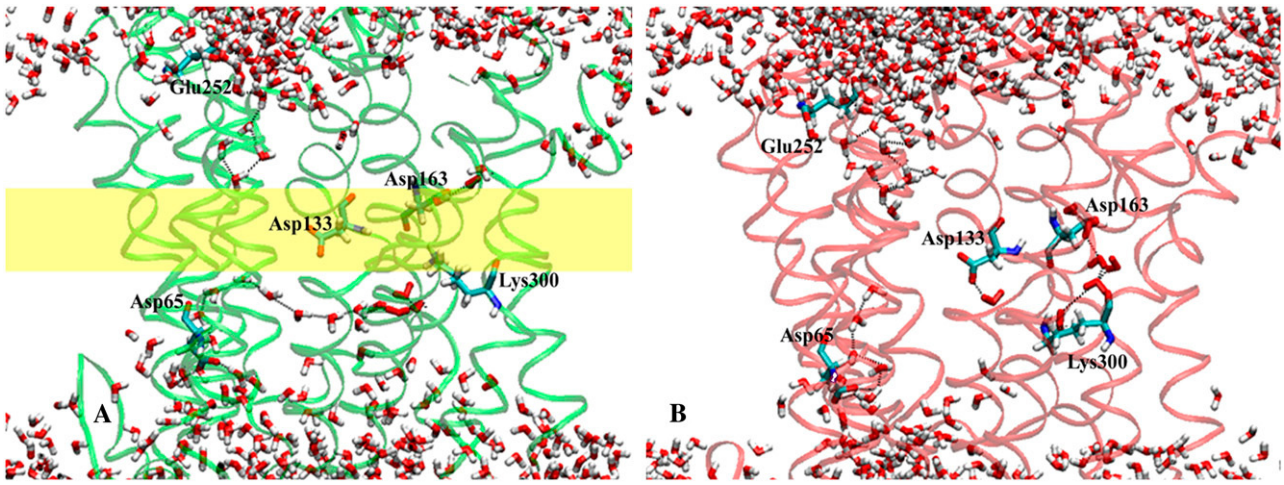

FIGURE 5 Plot of residues forming hydrogen bonds with water molecules for the simulations at (*A*) pH 4 and at (*B*) pH 8. A hydrophobic barrier between the cytoplasmic and periplasmic funnels (*A*, *yellow*) is removed (*B*).

water molecule W_G7, and Lys^{300} forms a hydrogen bond with water molecule W_G10 (92% and 59% occupancy, respectively). However, at pH 8, Lys^{300} undergoes a significant reorientation of its uncharged side chain and forms hydrogen bonds with water molecules W_G7 and W_G10 (11% and 13% occupancy). The different values of occupancies of hydrogen bonds between water molecules and Lys^{300} in the simulations, at the different pH values, suggest that the protonation state of Lys^{300} has an effect on water ordering in the antiporter. One could also speculate that water molecule W_G7 may be of structural and functional importance because it contributes to the connection between helix X and the sodium binding site. A big shift was observed in the distance between the OD2 atom of Asp^{133} and the NZ atom of Lys^{300} from 9.21 Å at pH 4 to 7.18 Å at pH 8. In line with these results, a pH-dependent relocation of a proton between water molecule W_G7 and Lys^{300} was predicted earlier by MCCE calculations (10). Taken together, these pH-induced differences might result from penetration of water into this region, which would significantly alter the pK_a values of several titratable residues.

Simulations of a NhaA variant G338S that is pH independent

It is known from experimental studies that mutations of conserved residues in helix XI of NhaA affect the pH response (5). Extensive cross-linking data are in accordance with the close proximity between the TMSs of the IV/XI assembly and their crucial role for activity and pH regulation (32,33). A most informative example is the mutation G338S (34) in the TMS XI (Fig. 6 *B*), which completely removes the pH control and produces a NhaA variant fully active in a pH-independent manner. Because our biochemical data were obtained at the physiological pH range (pH 7–8.5), we produced MD trajectories for the variant at pH 8 and compared the results with the wild-type trajectories at pH 4 and pH 8. The variant simulation at pH 8 as compared with the simulation of the wild type at pH 4 shows that helix XIp remains in the same position as observed for the wild-type antiporter, whereas helix XIc moves toward helix X (Fig. 6 *A*). Strikingly, compared with the wild-type simulation at pH 8, the mutation G338S directly stabilizes a nonkink conformation of helix X, in contrast to the kinked helix X in the wild-type simulation at alkaline pH (Fig. 6 *A*).

Results from the trajectory analysis, based on the variant model, hint at an important role of water molecules buried among the sodium binding site, helix XI, and helix X. These water molecules affect the conformational dynamics of NhaA. In the variant structure, four water molecules, located between residue Ser^{338} and Asp^{163} form a stable chain, connecting these residues for the entire duration of the simulation (Fig. 6 *B*). One of these water molecules, W_G9, is also hydrogen bonded to Lys^{300} of helix X. Therefore, we conclude that the existence of a hydrogen-bonded chain between residue Ser^{338} and Lys^{300} does not allow helix X to move freely or to change its conformation in response to variation in pH. In other words, the G338S variant can no longer respond to pH changes. One has to keep in mind that in the simulation procedure used here, we always started with an inactive low-pH conformation, and without a sodium ion in the putative sodium binding site. The fact that in the G338S variant our simulation does not show the conformational changes on increasing the pH as does the wild type could mean either that the conformational transition is prevented or that the pH sensing is lost in this variant. We prefer the first alternative, implying that helix X is a very important element for transition of the NhaA from low pH to the high-pH active state.

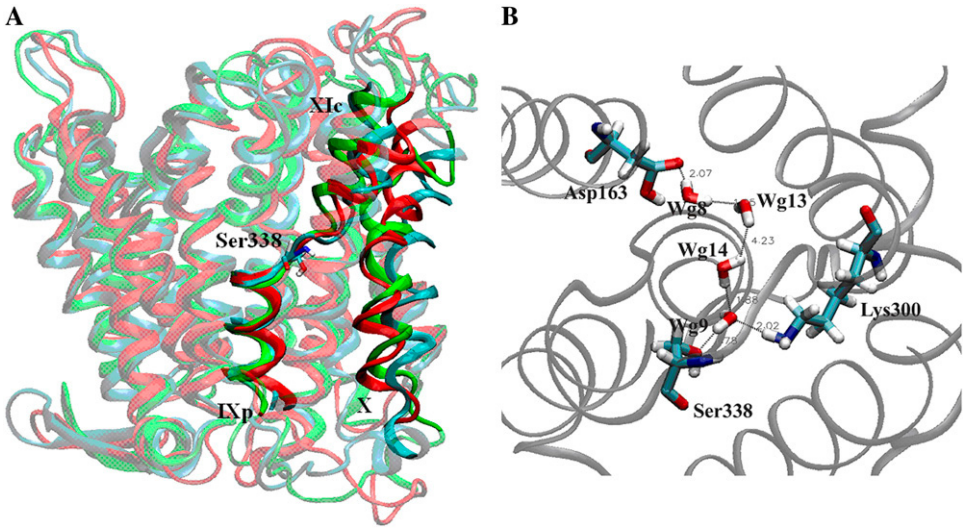

FIGURE 6 (*A*) Superimposition of the NhaA antiporter atomic models at pH 4 (shown in *green*) and at pH 8 (shown in *red*) for the wild type and for the mutant at pH 8 (shown in *cyan*) after 2.0 ns of molecular dynamics production. (*B*) The hydrogen-bonding interactions of Ser^{338}, Asp^{163}, and Lys^{300} residues in the mutant structure of NhaA antiporter G338S. The backbone atoms are indicated by gray.

Limitations of the current approach

It is necessary to mention several limitations of the simulation approach used in this study. The main limitation is that the structure of the antiporter exists only in the closed conformation. Second, there is no sodium ion in the sodium binding site. Third, a time scale of ~4 ns simulates only the initial steps of activation of the NhaA antiporter. However, we think that our simulations identify flexible structural elements that appear to be involved in the initial steps of the pH-induced activation process of NhaA and provide hints to further experiments.

CONCLUSIONS

We performed MD simulations on the basis of the acidic pH locked crystal structure of NhaA. Analysis of the stability of the simulated systems at pH 4 and pH 8 shows that the α-helical regions preserve the general architecture of NhaA throughout the pH change. In contrast, large conformational drifts occur in the loop regions at pH 8.

The time-dependent fluctuations imply an increased flexibility of helix IVp on shifting the pH from 4 to 8.

A comparison of the MD simulations of helix X at pH 4 and pH 8 reveals a remarkable pH-induced conformational reorganization; in line with the x-ray crystallographic data and the simulations at acidic pH, helix X is slightly curved at acidic pH. However, at alkaline pH, helix X acquires a kinked conformation around residue Lys^{300}.

Constructing and analyzing the dynamic hydrogen-bonded network reveal, in line with the structural data, a hydrophobic barrier between the cytoplasmic and periplasmic funnels of NhaA at acidic pH. The simulation at pH 8 shows that this barrier is removed, and two funnels are bridged by hydrogen bonds between water molecules and residues located in the TMSs IV/XI assembly and helix X. For example, penetration of water molecules and structural reorganizations significantly alter the distance between Lys^{300} and the Na^+ binding site at alkaline pH.

MD simulations of the variant G338S at alkaline pH explain its loss of pH control; the formation of a hydrogen-bonded chain between residues Ser^{338} and Lys^{300} does not allow helix X to move freely and to acquire the kinked configuration that is needed for pH regulation.

The authors thank Prof. Volkhard Helms (Saarbrücken) for critically reading the manuscript, Lena Kozachkov and Katia Herz (Alexander Silberman Institute of Life Science, Hebrew University) for the discussion, and Dr. Matthias Appel and Prof. Werner Kühlbrandt (Max Planck Institute of Biophysics) for sharing unpublished results.

This work was supported by the Deutsche Forschungsgemeinschaft (SFB 472), the Fonds der Chemischen Industrie, the Max-Planck-Gesellschaft, the German Israeli Foundation for Scientific Research and Development (to H.M. and E.P.), and the Israeli Science Foundation (E.P.).

REFERENCES

1. Padan, E., and S. Schuldiner. 1994. Molecular physiology of Na^+/H^+ antiporters, key transporters in circulation of Na^+ and H^+ in cells. *Biochim. Biophys. Acta*. 1185:129–151.
2. Padan, E., M. Venturi, Y. Gerchman, and N. Dover. 2001. Na(+)/H(+) antiporters. *Biochim. Biophys. Acta*. 1505:144–157.
3. Padan, E., E. Bibi, M. Ito, and T. A. Krulwich. 2005. Alkaline pH homeostasis in bacteria: new insights. *Biochim. Biophys. Acta*. 1717: 67–88.
4. Taglicht, D., E. Padan, and S. Schuldiner. 1993. Proton-sodium stoichiometry of NhaA, an electrogenic antiporter from *Escherichia coli*. *J. Biol. Chem*. 268:5382–5387.
5. Padan, E., T. Tzubery, K. Herz, L. Kozachkov, A. Rimon, and L. Galili. 2004. NhaA of *Escherichia coli*, as a model of a pH-regulated Na^+/H^+ antiporter. *Biochim. Biophys. Acta*. 1658:2–13.
6. Hunte, C., E. Screpanti, M. Venturi, A. Rimon, E. Padan, and H. Michel. 2005. Structure of a Na^+/H^+ antiporter and insights into mechanism of action and regulation by pH. *Nature*. 435:1197–1202.
7. Putney, L. K., S. P. Denker, and D. L. Barber. 2002. The changing face of the Na^+/H^+ exchanger, NHE1: structure, regulation, and cellular actions. *Annu. Rev. Pharmacol. Toxicol*. 42:527–552.

8. Wakabayashi, S., T. Pang, T. Hisamitsu, and M. Shigekawa. 2003. Two functional regulatory factors of the Na^+/H^+ exchangers. *In* The sodium-hydrogen exchanger: from molecule to its role in disease. M. Karmazyn, M Avkiran, L. Fliegel, editors. Kluwer Academic Publishers, Boston, MA. 35–49.

9. Goodford, P. J. 1985. A computational procedure for determining energetically favorable binding sites on biologically important macromolecules. *J. Med. Chem.* 28:849–857.

10. Olkhova, E., C. Hunte, E. Screpanti, E. Padan, and H. Michel. 2006. Multiconformation continuum electrostatics analysis of the NhaA Na^+/H^+ antiporter of *Escherichia coli* with functional implications. *Proc. Natl. Acad. Sci. USA.* 103:2629–2634.

11. Gunner, M. R., and E. Alexov. 2000. A pragmatic approach to structure based calculation of coupled proton and electron transfer in proteins. *Biochim. Biophys. Acta.* 1458:63–87.

12. Venturi, M., A. Rimon, Y. Gerchman, C. Hunte, E. Padan, and H. Michel. 2000. The monoclonal antibody 1F6 identifies a pH-dependent conformational change in the hydrophilic NH(2) terminus of NhaA Na(+)/H(+) antiporter of *Escherichia coli*. *J. Biol. Chem.* 275:4734–4742.

13. Gerchman, Y., A. Rimon, and E. Padan. 1999. A pH-dependent conformational change of NhaA Na(+)/H(+) antiporter of *Escherichia coli* involves loop VIII–IX, plays a role in the pH response of the protein, and is maintained by the pure protein in dodecyl maltoside. *J. Biol. Chem.* 274:24617–24624.

14. Tzubery, T., A. Rimon, and E. Padan. 2004. Mutation E252C increases drastically the K_m value for Na^+ and causes an alkaline shift of the pH dependence of NhaA Na^+/H^+ antiporter of *Escherichia coli*. *J. Biol. Chem.* 279:3265–3272.

15. Brooks, B. R., R. E. Bruccoleri, B. D. Olafson, D. J. States, S. Swaminathan, and M. Karplus. 1983. CHARMM: a program for macromolecular energy minimization and dynamics calculations. *J. Comput. Chem.* 4:187–217.

16. MacKerell, A., Jr., J. Wiorkiewicz-Kuczera, and M. Karplus. 1995. An all-atom empirical energy function for the simulation of nucleic acids. *J. Am. Chem. Soc.* 117:11946–11975.

17. MacKerell, A. D., Jr., D. Bashford, M. Bellot, R. L. Dunbrack, J. D. Evanseck, M. J. Field, S. Fischer, J. Gao, H. Guo, D. Joseph-McCarthy, S. Ha, L. Kuchnir, K. Kuczera, F. T. K. Lau, C. Mattos, S. Michnick, T. Ngo, D. T. Nguyen, B. Prodhom, W. E. Reiher, B. Roux, M. Schlenkrich, J. Smith, R. Stote, J. Straub, M. Watanabe, J. Wiorkiewicz-Kuczera, and M. Karplus. 1998. All-atom empirical potential for molecular modeling and dynamics studies of proteins. *J. Phys. Chem. B.* 102:3586–3616.

18. Berneche, S., M. Nina, and B. Roux. 1998. Molecular dynamics simulation of melittin in a dimyristoylphosphatidylcholine bilayer membrane. *Biophys. J.* 75:1603–1618.

19. Woolf, T. B., and B. Roux. 1996. Structure, energetics, and dynamics of lipid-protein interactions: A molecular dynamics study of the gramicidin A channel in a DMPC bilayer. *Proteins.* 24:92–114.

20. Berneche, S., and B. Roux. 2000. Molecular dynamics of the KcsA K(+) channel in a bilayer membrane. *Biophys. J.* 78:2900–2917.

21. Essmann, U., L. Perera, M. L. Berkowitz, T. Darden, H. Lee, and L. G. Pedersen. 1995. A smooth particle mesh Ewald method. *J. Chem. Phys.* 103:8577–8593.

22. Ryckaert, J. P., G. Ciccotti, and H. J. C. Berendsen. 1977. Numerical integration of the Cartesian equation of motions of a system with constraints: molecular dynamics of *n*-alkanes. *J. Comp. Chem.* 23:327–341.

23. Schlenkrich, M. J., J. Brickmann, Jr., A. D. MacKerell, and M. Karplus. 1996. An empirical potential energy function for phospholipids: criteria for parameter optimization and applications. *In* Biological Membranes. A Molecular Perspective from Computation and Experiment. K. M. Merz, and B. Roux, editors. Birkhäuser, Boston. 31–81.

24. Jorgensen, W. L., J. Chandrasekhar, J. D. Madura, R. W. Impey, and M. L. Klein. 1983. Comparison of simple potential functions for simulating liquid water. *J. Chem. Phys.* 79:926–935.

25. Visiers, I., B. B. Braunheim, and H. Weinstein. 2000. ProKink: a protocol for numerical evaluation of helix distortions by praline. *Protein Eng.* 13:603–606.

26. Tang, Y., and L. Nilsson. 1999. Molecular dynamics simulations of the complex between human U1A protein and hairpin II of U1 small nuclear RNA and of free RNA in solution. *Biophys. J.* 77:1284–1305.

27. Humphrey, W., A. Dalke, and K. Schulten. 1996. VMD: visual molecular dynamics. *J. Mol. Graph.* 14:27–28, 33–38.

28. Luecke, H. 2000. Atomic resolution structures of bacteriorhodopsin photocycle intermediates: the role of discrete water molecules in the function of this light-driven ion pump. *Biochim. Biophys. Acta.* 1460:133–156.

29. Brandl, C. J., and C. M. Deber. 1986. Hypothesis about the function of membrane-buried proline residues in transport proteins. *Proc. Natl. Acad. Sci. USA.* 83:917–921.

30. Sansom, M. S., and H. Weinstein. 2000. Hinges, swivels and switches: the role of prolines in signalling via transmembrane alpha-helices. *Trends Pharmacol. Sci.* 21:445–451.

31. Ulmschneider, M. B., D. P. Tieleman, and M. S. Sansom. 2005. The role of extra-membranous inter-helical loops in helix-helix interactions. *Protein Eng. Des. Sel.* 18:563–570.

32. Galili, L., A. Rothman, L. Kozachkov, A. Rimon, and E. Padan. 2002. Trans membrane domain IV is involved in ion transport activity and pH regulation of the NhaA-Na(+)/H(+) antiporter of *Escherichia coli*. *Biochemistry.* 41:609–617.

33. Galili, L., K. Herz, O. Dym, and E. Padan. 2004. Unraveling functional and structural interactions between transmembrane domains IV and XI of NhaA Na^+/H^+ antiporter of *Escherichia coli*. *J. Biol. Chem.* 279: 23104–23113.

34. Rimon, A., Y. Gerchman, Z. Kariv, and E. Padan. 1998. A point mutation (G338S) and its suppressor mutations affect both the pH response of the NhaA-Na^+/H^+ antiporter as well as the growth phenotype of *Escherichia coli*. *J. Biol. Chem.* 273:26470–26476.